Depth of penetration of bubbles entrained by an oscillated plunging water jet

Grégory Guyot, Alain H. Cartellier, Jean-Philippe Matas

Depth of penetration of bubbles entrained by an oscillated plunging water jet

Grégory Guyot[a,b,*], Alain Cartellier[a], Jean-Philippe Matas[c]

[a] *Université Grenoble Alpes, CNRS, Grenoble INP, LEGI, F-38000 Grenoble, France*
[b] *EDF-CIH, F-73330 Le Bourget du Lac, France*
[c] *Laboratoire de Mécanique des Fluides et d'Acoustique, Ecole Centrale de Lyon, CNRS, Université Claude Bernard Lyon 1, INSA Lyon, F-69134 Ecully, France*

Abstract

We present experimental measurements of the penetration depth of the bubble cloud generated by a plunging water jet, when this jet is oscillated parallel to the free surface. We demonstrate that when the Reynolds number is larger than 10^4 the penetration depth can be adequately described with the model introduced by Clanet & Lasheras (1997) for a non-oscillating jet tilted relative to the normal of the liquid surface, provided an effective inclination angle is introduced to account for the jet translation velocity. In the case of jets with a Reynolds number smaller than 10^4, we find that the penetration depth of the oscillated jet can be increased of up to 30% by moderate oscillation velocities. This increase of the penetration is due to the decrease of the mixing layer angle when the symmetry around the bubble cloud is broken by the oscillation. We finally discuss the shape of the overall region impacted by the oscillating bubble cloud. We show that there is a regime for which the penetration is maximum at the center of this region, and a regime for which the penetration is maximum at the periphery. We propose a cartography to predict when each regime is relevant.

Keywords: bubbly flow, oscillating jet, depth of penetration, jet impact, aeration, coherent jet

1. Introduction

Air entrainment due to high-speed liquid structures such as drops, jets or waves impacting a free surface is commonly encountered in nature, e.g. cascades or breaking waves (Deike et al. (2016)), as well as in industry (Chanson et al. (2006); Pagliara et al. (2011); Duarte et al. (2016); Descloux et al. (2016)). It is notably present in environmental engineering (e.g. aeration), for process control (e.g. foam destruction) or in energy production (dams, turbines). Air entrainment involves various elementary processes such as bubble formation mechanisms, bubble transport mechanisms beneath the free surface which have been investigated in diverse situations. Extensive reviews of our current understanding of air entrainment by plunging jets have been proposed by Biń (1993), Kiger & Duncan (2012) and more recently Miwa et al. (2018).

*. Corresponding author
Email address: gregory.guyot@edf.fr (Grégory Guyot)

In this article, we focus on the penetration depth reached by the bubble cloud entrained by a cylindrical liquid jet plunging into a pool of the same fluid. Many semi empirical relations or empirical relations have been proposed to predict this penetration depth. The most popular are reported in table 1, and include those of McKeogh & Ervine (1981), Falvey & Ervine (1987), Nakasone (1987) and Ohkawa et al. (1986) among others. Note that the dimensional correlations proposed by McKeogh & Ervine (1981), and by Ohkawa et al. (1986) are given in S.I. units. Yet, and as discussed in the above-mentioned reviews, there is no clear consensus on the prevailing parameters and on the relevant scaling laws for predicting the penetration depth. This situation is probably due to the variety of configurations to be accounted for in terms of jet topology at impact which range from smooth to rough and up to fully destabilized depending on the size and the velocity of the jet. The nature of the initial disturbances (including the turbulence in the liquid, secondary flows etc.) and the distance between the injector and the free surface are also expected to impact the bubble cloud dynamics. In this context, our objective is to investigate the influence of a specific disturbance consisting in an oscillation of the liquid jet parallel to the free surface. Such oscillations are indeed observed to occur along falling jets, notably when the distance between the injector and the free surface is not too small (Guyot et al. (2016)). In order to isolate the effect of oscillations from other kinds of perturbations, we consider turbulent water jets of small diameter and with moderate interfacial corrugations. These types of jets have been investigated by Clanet & Lasheras (1997) for jet diameters up to a few millimeters and using long needles as injectors (length to diameter ratios larger than 50) in order to ensure fully developed turbulent flows. Moreover, these authors have established a predictive model for the penetration depth which proves valid over a large range of injection velocities. The control parameters in this model are the jet diameter, the jet velocity at the nozzle, the terminal bubble velocity, the spread angle of the bubble cloud and the jet inclination with respect to the free surface. We will investigate similar jets but with a vertical needle oscillating above the free surface and parallel to it. We will show how the Clanet & Lasheras (1997) model can be adapted when the liquid jet is mobile. We first present the experimental method in the next section. The experimental results and their interpretation will be presented in the following section.

2. Experimental method

A round water jet issued from a nozzle of diameter D at a mean outlet velocity V_0 falls into an overflowing cubic reservoir (edge 50 cm). The distance h between the tip of the nozzle and the water surface is constant for a given nozzle diameter : as in Clanet & Lasheras (1997), the ratio h/D was kept constant and equal to 20. The ratio of the maximum penetration depth to the total depth never exceeded 0.30, in order to minimize the effect of the finite size of the pool. All nozzles are stainless steel needles with length to diameter ratios L_0/D larger than 50. The exit velocity profile can then be assumed to be fully developed. A water circuit delivers a steady flow rate at the nozzle via a pressure regulator. A 10 microns water filter has been inserted upstream of the circuit to clear the water. The flow rate is measured with a flowmeter located just above the nozzle. The flow rate range for our experiments is from 6.10^{-4} l/s to 3.10^{-2} l/s, with an overall uncertainty of 5%. The nozzle, which remains vertical in all our experiments, is attached to a vibration table

Table 1: Examples of correlations for the penetration depth H

McKeogh & Ervine (1981)	$H = 2.6(V_0 D)^{0.7}$	V_0 : velocity at injection D : nozzle diameter
Falvey & Ervine (1987)	$H/d_i = 3.1Q/Q_i$	Q : water discharge Q_i : jet water discharge at impact d_i : jet diameter at impact
Nakasone (1987)	$H = (2/3)h$	h : distance between tip of the nozzle and water surface
Ohkawa et al. (1986)	$H = 5.5(V_0 D)^{0.73}(h/D)^{-0.26}(\cos\theta)^{1.11}$	θ : jet inclination angle (from vertical)

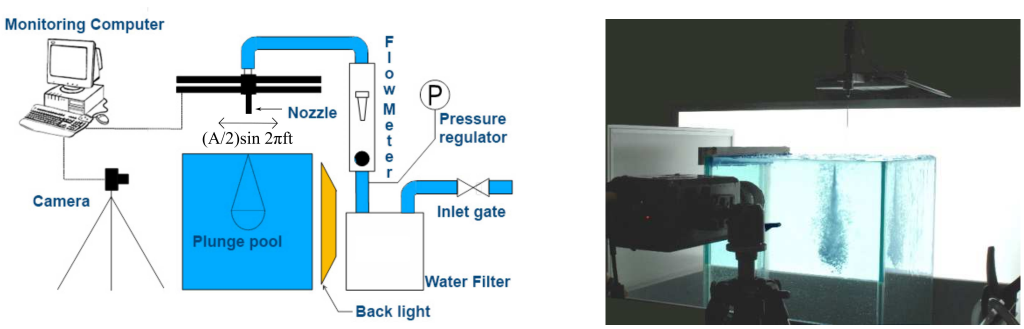

(a) (b)

Figure 1: Sketch and view of the experimental apparatus. The nozzle is oscillated parallel to the interface with a peak to peak amplitude A and frequency f.

controlled by a computer. This lab-made vibration table consists in a metal plate driven by a linear motor, guided by bearings. The jet behavior under the water surface can be captured by two cameras : a Nikkon D200 (3872 pixels by 2592 pixels) or a Phantom V10 (1280 pixels by 720 pixels, 1016 frames per seconds) monitored by the same computer. The lens used with these cameras is a Nikon AF Nikkor 50 mm f/1.8D. Figure 1 illustrates the set-up : note in particular on figure 1 right that the reservoir is slightly tilted to the right, so that it overflows over a single lateral wall without perturbing visualization.

Three nozzle diameters were tested, D =2.4 mm, 1.3 mm, and 0.3 mm. The velocity range is 1.9 m/s to 20.1 m/s. We introduce the Reynolds number $Re = V_0 D/\nu$ and Weber number $We = \rho V_0^2 D/\sigma$, where ν is water kinematic viscosity, ρ the water density and σ the surface tension of water. For our experiments at $T = 20°C$, values of Re and We are computed with $\nu = 10^{-6}$ m^2/s, ρ=1000 kg/m^3 and $\sigma = 0.072$ N/m. The values of D and V_0 used in our experiments and the corresponding values of Re and We are reported on table 2. The Reynolds number range is 2420

TABLE 2: Values of D, V_0, Re and We for our experiments

Internal Nozzle Diameter D (mm)	Nozzle outlet velocity V_0 (m/s)	Reynolds Number Re	Weber number We
2.4	1.89	4525	117
2.4	2.92	7011	281
2.4	3.88	9315	497
2.4	5.04	12104	839
2.4	6.76	16228	1507
2.4	7.22	17319	1717
1.3	1.86	2420	62
1.3	5.65	7345	570
1.3	8.41	10928	1262
1.3	12.2	15853	2656
1.3	15.6	20331	4368
1.3	18.6	24137	6156
0.3	9.83	2949	398
0.3	11.8	3540	574
0.3	14.9	4486	921
0.3	20.0	6022	1661

to 24100 whereas the Weber number range is 62 to 6150.

The displacement imposed by the vibration table along the axis of its linear motor is a sinusoid $A/2\sin(2\pi f t)$. The metal plate entrained by the motor, to which the nozzle is attached, moves parallel to the reservoir surface. The values of peak-to-peak amplitude A and frequency f for our experiments are shown in table 3. The motion of the vibration table was recorded with high speed imaging before each measurement series in order to check i) that the difference between the actual displacement amplitude and the prescribed amplitude never exceeded 5% ii) that the motion was harmonic, and that the frequency of the motion was close enough to the prescribed frequency (the maximum measured difference was 0.1 Hz). The values of D, V_0, A and f in tables 2 and 3 correspond to a total of 848 different experimental conditions.

A minimum of 50 pictures were recorded for each velocity/diameter/amplitude/frequency condition, at a low sampling frequency of 1 Hz : the time between two images is therefore much larger than the typical time of flight H/V_0, and this ensures that two consecutive images are relatively independent, which accelerates convergence of average quantities. The penetration depth of the bubble cloud was experimentally measured, applying a grey gradient analysis

Table 3: Values of amplitude A and frequency f tested in our experiments.

Amplitude A (mm)	Frequency f (Hz)														
	0	1	2	5	7.5	10	12.5	15	17.5	20	22.5	25	27.5	30	32.5
2.5	x	x	x	x	x	x	x	x	x	x	x	x	x	x	x
4	x	x	x	x	x	x	x	x	x	x	x	x	x		
8	x	x	x	x	x	x	x	x	x	x					
12	x	x	x	x	x	x	x	x	x						
16	x	x	x	x	x	x									

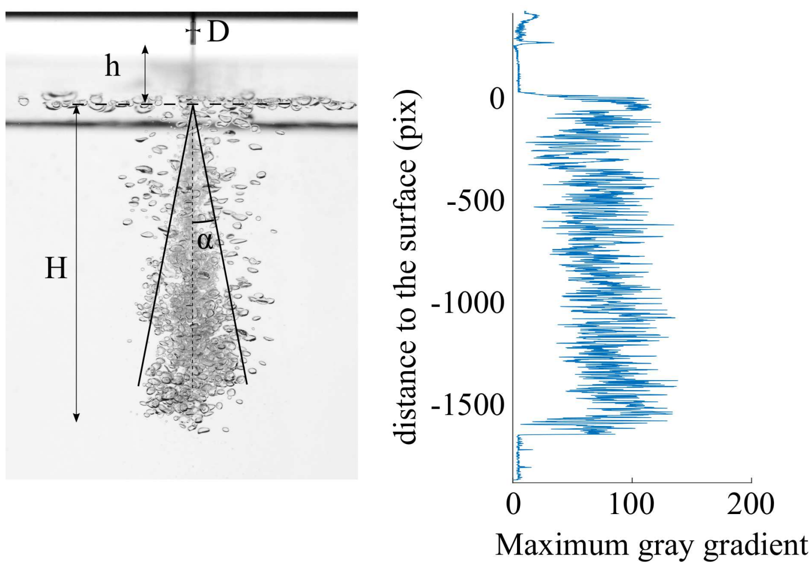

Figure 2: Sample picture of a plunging jet and corresponding values of the maximum vertical gray gradient for each depth. The angle α is the angle of the mixing layer of the liquid jet, which is assumed to be constant in the model.

on each sample image (such as figure 2) : starting from the bottom of the image i) For a given line on the image a vertical gradient of gray level is computed for each horizontal position; ii) The maximum value of this gradient is retained for the given line. The values of these maxima are plotted on figure 2 for each line. It can be seen on figure 2 that the lower limit of the first bubble corresponds to a very steep increase of the maximum gradient; iii) The depth where this maximum gradient becomes larger than a fixed threshold is retained as the bubble cloud edge. The distance from this edge to the location of the free surface at rest (marked by a dashed line on figure 2) is computed for each set of 50 pictures, and given V_0, D, A and f : we note H the average of these 50 values. The chosen number of 50 pictures is largely sufficient to ensure convergence of H for our conditions. The overall uncertainty for these penetration depth measurements is 10%.

3. Experimental results and discussion

3.1. Bubble penetration depth for a non-oscillating jet

First of all, our experimental results were compared to the model proposed by Clanet & Lasheras (1997) for a steady plunging jet normal to a flat liquid surface. This simple model is based on the idea that bubbles will be entrained downwards by the liquid jet until the liquid jet velocity reaches U_T, the terminal bubble velocity. The liquid velocity U as a function of depth z can be estimated from momentum conservation, and by assuming that the liquid jet widens with a constant half angle α. As demonstrated in Maxworthy et al. (1996) there is a minimum terminal velocity $U_T = 0.22$ m/s for bubbles over 1 mm diameter in water. The size of the bubble cloud is therefore directly deduced from the depth where liquid velocity reaches U_T. Writing that $U(z) = V_0 D/D_z$ where D_z is the diameter of the liquid jet at depth z, we find that velocity U_T is reached at a depth $V_0 D/(2U_T \tan\alpha)$. The depth H_1 predicted by this model is then :

$$\frac{H_1}{D} = \frac{1+\tan\alpha}{2\tan\alpha}\frac{V_0}{U_T} \tag{1}$$

Clanet & Lasheras (1997) propose a constant value of $\alpha = 12.5°$ for all their measurements : this assumption is

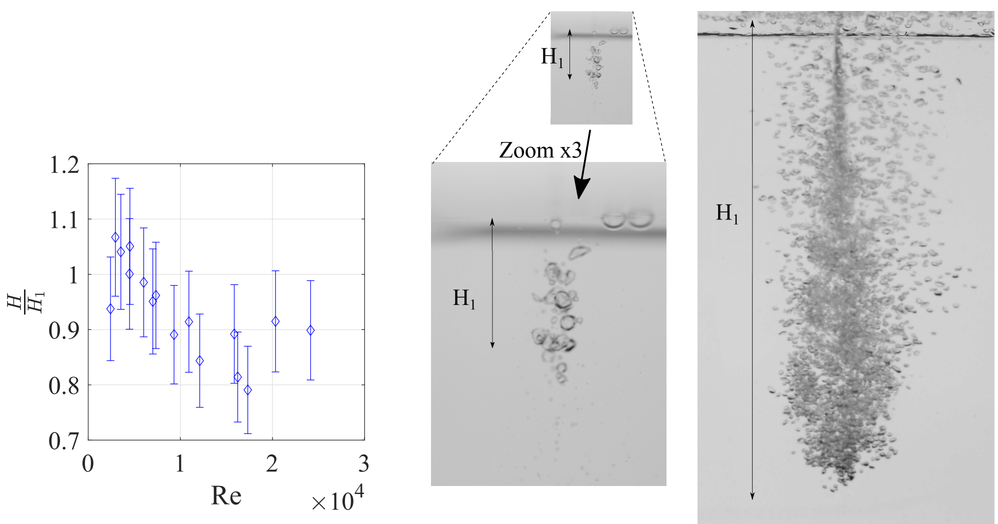

a) b) c)

FIGURE 3: a) Ratio of measured penetration depth to the model of Clanet and Lasheras (1997), for the case of a non-oscillating jet. The error bar corresponds to a 10% uncertainty on the measurement of H. b) Image of the bubble cloud for $D_0 = 1.3$ mm, $V_0 = 1.86$ m/s (top : same scale as in image c) ; bottom : magnified x3) : the predicted penetration depth $H_1 = 3.0$ cm is in agreement with the size of the bubble cloud ; c) Same nozzle, but $V_0 = 18.6$ m/s. Predicted $H_1 = 30$ cm is again in agreement with the size of the bubble cloud.

obviously a strong one, because α is actually expected to vary spatially as the liquid jet slows down and bubbles escape the jet near its bottom. We estimate the value of this (assumed constant) angle α for our experiments by deducing it from the width of the entrained bubble cloud at the penetration depth (see figure 2). The average α measured for our experimental conditions is 11.8° with a standard deviation of 1.2° : this value is consistent with the value of 12.5° proposed by Clanet & Lasheras (1997), but slightly smaller than the value of $\alpha = 14°$ proposed by Ervine et al. (1997). We compare in figure 3a the result of measurements of the average penetration depth for a non-oscillating jet, H, to the model penetration depth H_1 as a function of the Reynolds number of the liquid jet Re. All diameters and outlet velocities of table 2 were tested. The error bars correspond to the amplitude of the temporal fluctuations of H, which are of the order of the jet width. These fluctuations, which arise possibly because of turbulence and because of the interaction with ascending bubbles, are the main cause of uncertainty, and largely overcome the uncertainty introduced by the image analysis. They are estimated at 10% of H. We observe on figure 3a that the ratio H/H_1 is close to one for all conditions, in spite of the strong assumption on the mixing layer angle. There is however an influence of the Reynolds number : for $Re > 10^4$, the model overestimates the measured length by 10%-20%. The correctness of the prediction of equation (1) indicates that considering the linear spreading of a single phase jet (Pope (2000); Horn & Thring (1956)) is an acceptable approximation even in the presence of entrained bubbles. One reason for this relies on the moderate void fractions involved in such situations which therefore induce a weak momentum transfer between phases and thus a weak modification of the jet dynamics. The fact that these void fractions are moderate can be qualitatively appreciated from instantaneous images (see figures 2,3b and c, and 8) as the optical density is never strong enough to fully block the light propagation. Quantitative data are also available in the literature (e.g. McKeogh & Ervine (1981); Van de Donk (1981)) which indicate that, in the quasi fully developed region, the void fraction is maximum on the center line. It starts from a value about 0.4 at most but it strongly decays with the distance d beneath the free surface (as d^{-3}) and it strongly decays radially. These features imply that the void fraction is significant only in a relatively small portion of the jet beneath the free surface. This feature is confirmed by the two-fluid simulations of Ma et al. (2010) that account for momentum transfer including drag, added mass, lift as well as turbulent dispersion contribution and that properly recover the experimental void fraction profiles at different distances beneath the free surface.

3.2. *Bubble penetration depth for an oscillating jet*

We now present measurements of H when the nozzle is oscillated parallel to the interface with an amplitude A and a frequency f. On figure 4, the dimensional bubble penetration depth is plotted as a function of f for all the conditions of tables 2 and 3. The $D = 0.3$ mm nozzle corresponds to the orange and red lines, the $D = 1.3$ mm nozzle to the yellow and green lines and the $D = 2.4$ mm nozzle to the the cyan and dark blue lines. For each D, five amplitude values are tested which is why five lines are represented for each series. A close-up of the data for $D = 0.3$ mm and lower H values is shown on figure 5. The first observation is that H spans a large range of values, from 9 mm to 271 mm, for all 848 experimental points. For most series, bubble penetration depth decreases when frequency is increased at constant D, V_0 and A. However, a maximum of penetration depth is measured for low frequencies (between 1 and 5 Hz) for several series : this occurs in particular for the smaller V_0, and is relatively more pronounced for the smaller diameter D (see close-up on figure 5). When the oscillation amplitude A is increased, the penetration depth generally decreases : an increase of penetration depth with amplitude is nonetheless observed for a few cases, namely just before the maximum in frequency when this maximum is sharp (see e.g. case $V_0 = 15$ m/s and $A = 8$ mm to 16 mm for $f < 2.5$ Hz on figure 5).

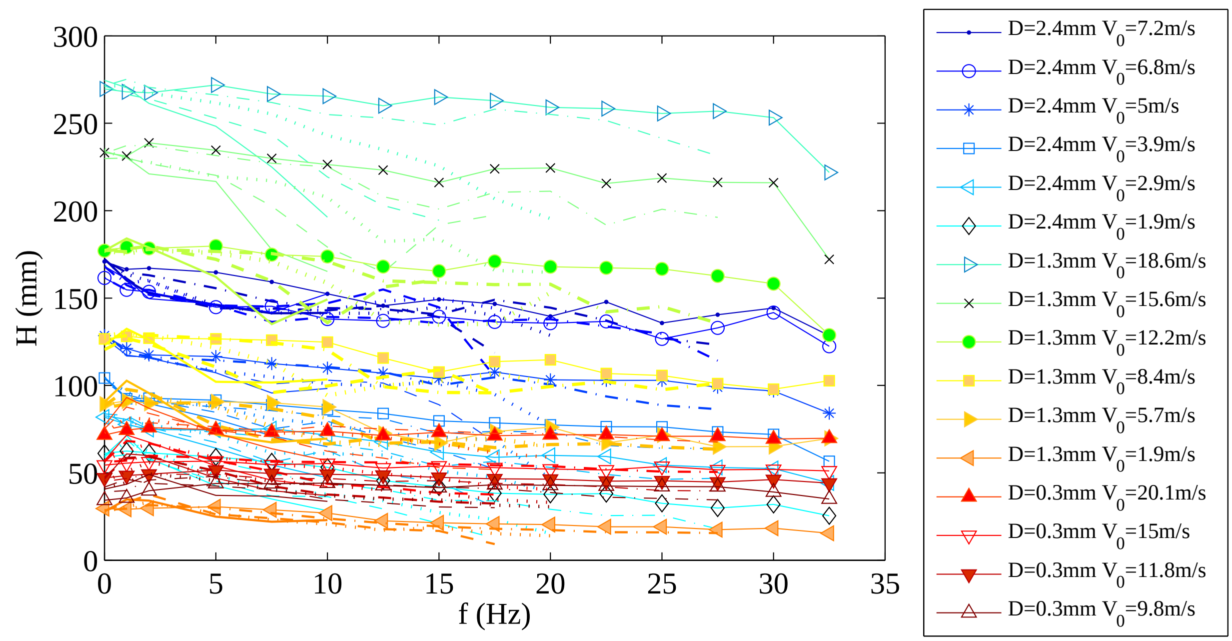

Figure 4: Bubble penetration depth H as a function of frequency f, for different D, V_0 and A. The orange and red lines correspond to the $D = 0.3$ mm nozzle, the yellow and green ones to the $D = 1.3$ mm nozzle and the cyan and dark blue ones to the $D = 2.4$ mm nozzle. Solid lines correspond to $A = 16$ mm, dashed lines to $A = 12$ mm, dotted lines to $A = 8$ mm, dash-dotted lines to $A = 4$ mm, and solid lines with symbol to A=2.5 mm.

3.2.1. Non dimensionalization of results

We now want to non-dimensionalize the results of figure 4. We first carry out a simple dimensional analysis : for the non-oscillating jet, the physical parameters of the problem are H, V_0, D, U_T. These parameters must be associated to two dimensionless numbers. Equation (1) gives H/D as a function of V_0/U_T, and as a function of α which is itself dimensionless. Figure 3 suggests that the Reynolds number (via the kinematic viscosity) should be introduced as a fourth dimensionless number. The oscillation of the jet introduces two additional physical parameters A and f. The amplitude can be non dimensionalized as A/D : the effect of A for fixed f will be discussed in section 3.2.4. In order to non dimensionalize frequency, we have to introduce a time scale. When frequency is increased, the horizontal velocity of the liquid jet relative to the surface increases. In a frame moving with the liquid jet, the situation is similar to that of a liquid jet entraining bubbles in an oscillating cross flow of characteristic velocity of order Af (the horizontal velocity is more precisely πAf with the definition of A introduced above). We therefore non dimensionalize frequency by introducing the velocity ratio associated to this situation, namely the ratio of horizontal velocity Af to vertical velocity. There are two vertical velocities in this problem : the initial jet velocity V_0, and the terminal velocity U_T

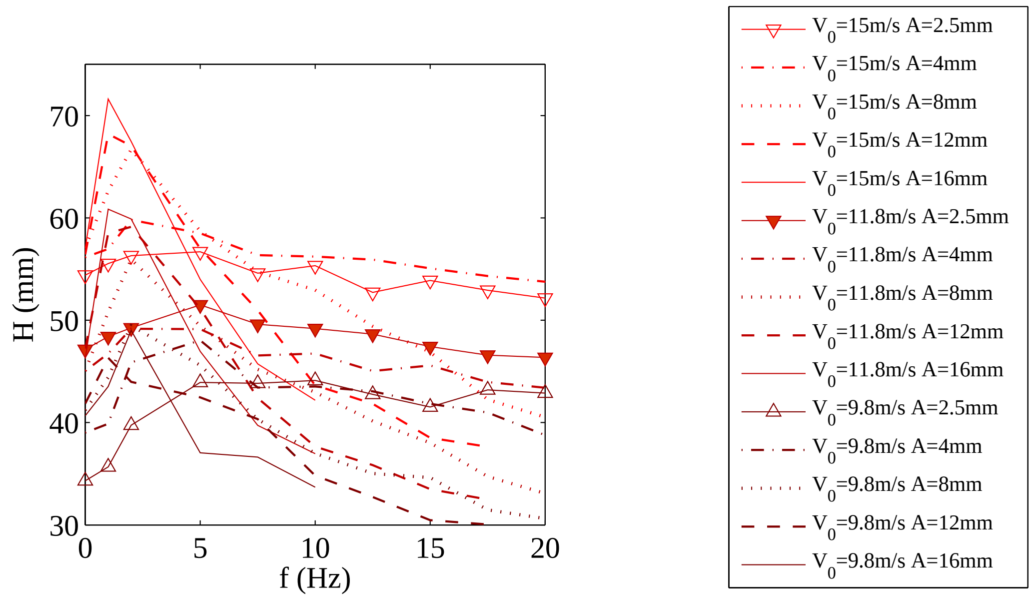

Figure 5: Bubble penetration depth H as a function of frequency f. Close-up on the data of figure 4 for diameter $D = 0.3$ mm and three smaller values of V_0. A maximum in penetration depth is observed when f is varied.

reached by the liquid at the bottom of the bubble cloud, and therefore two possible Strouhal numbers, Af/V_0 and Af/U_T. We compare on figure 6 how these two Strouhal numbers, Af/V_0 and Af/U_T succeed in capturing the location of the maximum of H observed at low frequencies for small diameters and lower V_0 series. In this graph, the measured bubble penetration depth is made non dimensional with the length H_1 of equation (1). A first observation on figure 6a is that values of Af/V_0 for our experiments are always smaller than 0.03 : horizontal velocity is negligible compared to V_0, meaning that the liquid jet remains almost vertical when it hits the water surface. Note also that while maxima on figure 6a are clearly scattered over a wide range of Af/V_0, the same maxima occur at a constant $Af/U_T \approx 0.1$ on figure 6b.

The ratio between the (maximum) horizontal jet velocity and the terminal vertical liquid velocity within the bubble cloud, Af/U_T, is directly related to the (maximum) angle of inclination of the bubble cloud at its bottom. The Clanet & Lasheras (1997) work precisely includes the case of a jet inclined of an angle θ relative to the vertical : their experimental penetration depth exhibits a maximum when θ is varied, and this maximum is in the same proportions as the one we observe when f is varied (up to plus 30% in depth on figure 6b). Instead of Af/U_T, we therefore introduce as a new parameter the angle $\beta = \text{atan}(\pi Af/2U_T)$, which can be interpreted as the angle of the bubble cloud relative to the vertical when its vertical velocity is $2U_T$. This angle is expected to be more representative of the average inclination of the bubble cloud than the maximum angle built with vertical velocity U_T, only reached at the tip of the cloud. We plot on figure 7 the ratio H/H_1 as a function of β. The scattered data of figure 4 is now relatively gathered around ratios H/H_1 close to one. While the existence of a maximum of H with the inclination angle θ is not explained in the work

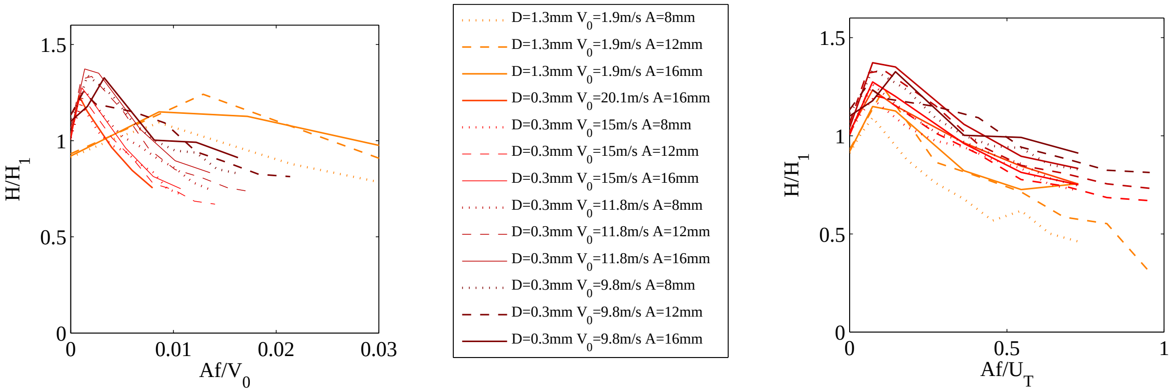

(a) (b)

Figure 6: Comparison of two possible Strouhal numbers in scaling the maximum in penetration depth : maxima occur for variable AF/V_0 (a), but for a constant $AF/U_T \approx 0.1$ (b).

of Clanet & Lasheras (1997), they propose a model for the decrease of H observed at large θ . This model, which is simply a geometrical variation of the model behind equation (1) when the jet is tilted, predicts a depth H_2 such that :

$$\frac{H_2}{D} = \frac{(1+\tan\alpha)\cos\theta + \tan\alpha\sin\theta}{2\tan\alpha}\frac{\cos(\theta-\alpha)}{\cos\alpha}\frac{V_0}{U_T} \qquad (2)$$

In this model it is assumed that the bubble cloud remains axisymmetric relative to the jet axis, namely that α does not depend on the azimuthal angle around the jet. The ratio H_2/H_1 is plotted as a dashed black line on figure 7, based on equation (2) with θ equated to β. Note that even though there is still a large dispersion around the prediction, the widely scattered data of figure 4 is relatively well gathered around the black curve. The model captures the decrease in penetration depth observed at larger horizontal velocities (equivalent to larger angles). The large dispersion of the experimental data around $\beta = 0.2 \pm 0.1$ rad (corresponding to $11^\circ \pm 6^\circ$) results from the fact that in this region some of the curves exhibit a maximum of H, while others decrease monotonically. Something is obviously missing in the model, and this is discussed in the next section.

3.2.2. *Existence of a maximum of penetration*

As mentioned above, a maximum in penetration depth of up to 30% is also observed by Clanet & Lasheras (1997) in their experimental data when they vary the angle of inclination θ of the jet, but it is not explained by their model. We first discuss this maximum observed when a non-oscillating inclined jet is inclined. Observation of the dynamics of the bubble cloud shows that when the jet is vertical and not oscillated, the bubbles released from the jet ascend all around the jet, figure 8a ; when the jet is slightly tilted, or equivalently when it is moving relative to the liquid bath because of an oscillation, the symmetry is broken and the bubbles ascend in a confined region farther from the plunging jet, see figure 8b. This has a strong impact on the angle α of the mixing layer : it can be seen on figure 8 that the value of α is larger when the bubbles ascend all around the jet. The angle α measured from these images is equal to 17° for figure

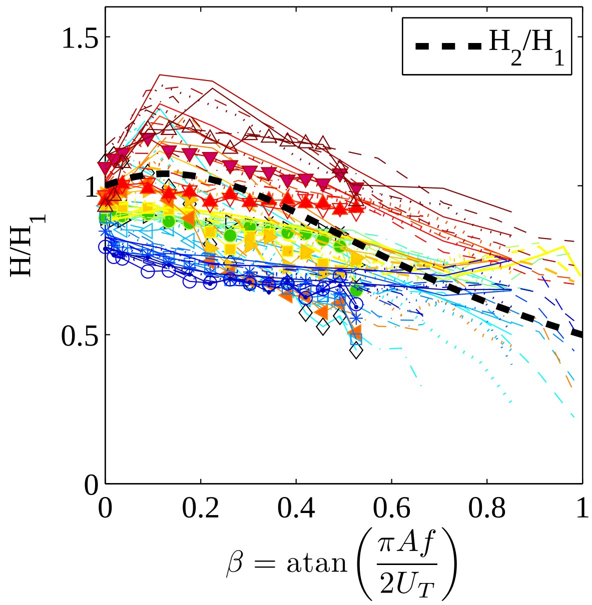

FIGURE 7: Non dimensional bubble penetration depth as a function of $\beta = \mathrm{atan}(\pi A f/2U_T)$. Same legend as in figure 4. Dashed black line corresponds to the model of Clanet and Lasheras (1997) for a jet tilted of an angle $\theta = \beta$, equation (2).

8a, and to 12° for figure 8b. We interpret the larger α of figure 8a as resulting from the annular upwards flow generated by ascending bubbles. When the jet is tilted, the ascending flow is displaced away from the plunging jet, α therefore decreases, which in turn leads to a larger penetration depth via momentum conservation (plus 30% on figure 8b).

This explains the existence of a maximum in the Clanet & Lasheras (1997) measurements when the jet inclination is increased. We believe the same mechanism explains the maximum observed in our experimental results. In other terms, for low but finite β, i.e. moderate horizontal velocities, the jet motion breaks the symmetry of the upwards flow and leads to a penetration larger than that for a vertical jet. If β is further increased (i.e. horizontal velocity further increased), the vertical penetration eventually decreases because a larger fraction of the jet momentum is injected in the horizontal direction, as modelled in equation 2.

As pointed out before, the maximum in penetration depth is not observed for all cases in figure 7. This maximum exists when $D = 0.3$ mm with all the velocities and Reynolds tested, whereas it only appears for velocities under 5.63 m/s (Re= 7345) for a nozzle diameter equal to $D = 1.3$ mm and only for the lowest velocity $V_0 = 1.88$ m/s (Re=4524) in the $D = 2.4$ mm case. Our interpretation is that when the momentum of the jet is larger, the impact of the bubble cloud on the liquid flow is smaller. We check this assumption by plotting on figure 9 the ratio of the maximum penetration depth when A and f are varied to the penetration depth H_0 when A and f are zero (•) as a function of the Reynolds number. There is a clear trend, namely this ratio decreases almost monotonically to one when *Re* is increased. The conditions for which no maximum is observed roughly correspond to Reynolds numbers larger than 10^4. Hence, an increase of the penetration depth with the oscillation of the jet can only be observed for low values

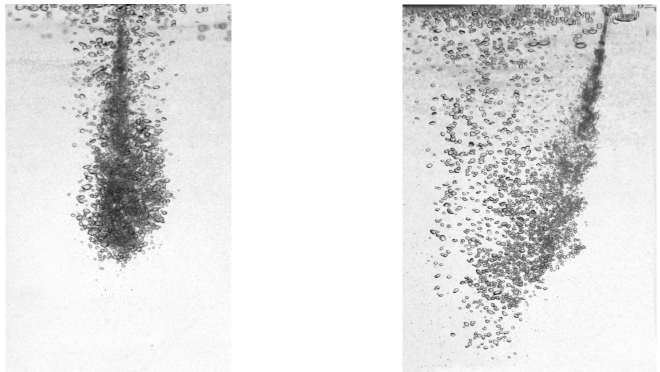

(a) (b)

Figure 8: Penetration cloud for D = 1.3 mm, V_0 = 15.64 m.s^{-1}, Re=20331 ; a) The nozzle is vertical ; b) The nozzle is tilted with an angle θ equal to 15.5°.

of Re, when the jet momentum is weaker. This increase can be of up to 30% for the smallest jet Reynolds numbers investigated, namely $Re \approx 2500 - 2900$. These values being close to the end of the transition to turbulence region, we can conclude that, for a oscillated fully turbulent jet, the maximum depth of penetration when Re is varied is 30% larger than the Clanet et al prediction. Note that we have not investigated laminar nor transition conditions for which the air entrainment process is changed.

We have also included on figure 9 three points corresponding to the data of Clanet and Lasheras (1997) : for these points the ratio H_{max}/H_0 corresponds to the ratio of the maximum penetration depth when the jet is inclined to the penetration depth when it is vertical for the same D and V_0. For a given Re the ratio H_{max}/H_0 observed in their experiment is larger than for our oscillated jet, but this is expected since the impact of the ascending secondary flow on H will be stronger when the jet is stationary than when its "effective inclination" oscillates. Interestingly, a decrease of H_{max}/H_0 with Re is also observed in their experiments.

3.2.3. Impact of mixing layer angle α on the penetration length

As mentioned in the preceding subsection, the existence of a maximum of penetration when the jet is oscillated is due to the impact of the oscillation on the mixing layer angle α. The model of Clanet & Lasheras (1997) is based on the assumption that α, the angle of the mixing layer, is constant. While this is mostly true for the case of the fixed jet, α is expected to exhibit strong variations when the jet is oscillated. We discuss in this paragraph these variations of α during the course of an oscillation of the liquid jet. We present some pictures of the bubble cloud along its oscillation on figure 10, for two distinct conditions : on the bottom line is represented the case where one of the highest maximum of H is measured on figure 5 (D = 0.3 mm, V_0 = 9.8 m/s, A = 12 mm, f = 1 Hz corresponding to Re = 2950) ; on the top line is a case without a maximum in penetration depth (D = 1.3 mm, V_0 = 18.6 m/s, A = 16 mm, f = 1 Hz corresponding to Re = 24137). For both lines the leftmost image shows the jet when it reaches its maximum excursion

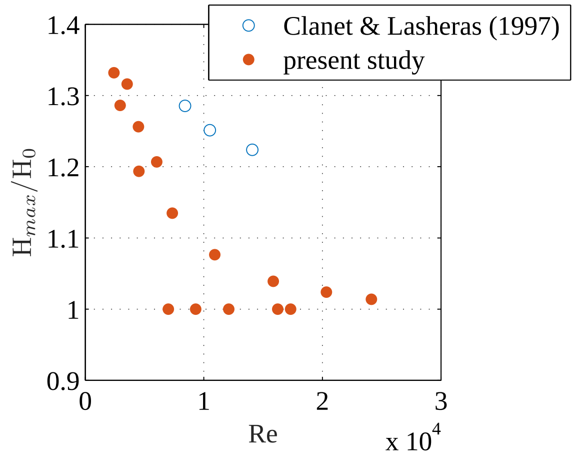

FIGURE 9: Ratio of maximum penetration depth H_{max} when A and f are varied, to penetration depth H_0 when $A = 0$ and $f = 0$, for fixed D and V_0, as a function of the Reynolds number : • present measurements, ○ Clanet and Lasheras (1997) measurements. The maximum is enhanced for low values of Re.

to the left, the central image represents the central position, corresponding to the maximum velocity ; the rightmost image the maximum excursion to the right. The numerical values correspond to an average of α measured on the left/right sides of the jet, and are deduced from the maximum width at the bottom of the cloud. When the jet of the bottom line is located at the extreme positions (left or right), α is around 7°, while it rises up to 11° when the jet is at the middle position (maximum velocity). On the contrary, no real variation of α happens for the conditions of the top line, for which no maximum of H was observed : α remains constant around 12°. The conditions of the top line of figure 10 correspond to a much larger Re than that of the bottom line, and our interpretation is that the constant α for this case results from the larger momentum of the liquid jet for these conditions. On the contrary, when Re is smaller as in the bottom line, the mixing layer angle of the jet is strongly impacted by the oscillation. Namely, the effect of the oscillation is to remove the jet from its ascending bubble cloud, leading to smaller values of α at the position of maximum amplitude.

Via the conservation of momentum, these local variations of α are expected to strongly impact the local penetration depth H_{loc}, defined as the instantaneous penetration depth observed at a given position : table 4 shows how a variation of α in the range 10-14° leads to variations of the model penetration depth H_1 of about 30%, via equation (1). A local decrease of the mixing layer angle at the outermost positions will therefore logically induce a larger local penetration depth at this location.

We believe the dispersion of the average penetration depth in figure 7 is caused by these variations of α, which are not accounted for in the Clanet & Lasheras (1997) model, only based on the assumption that $\alpha = 12.5°$. Namely we believe the difference between the red (small diameter D) and blue (large D) curves on figure 7 are the same as the difference between the top and bottom line on figure 10 : for a given amplitude/frequency if the jet has a much smaller

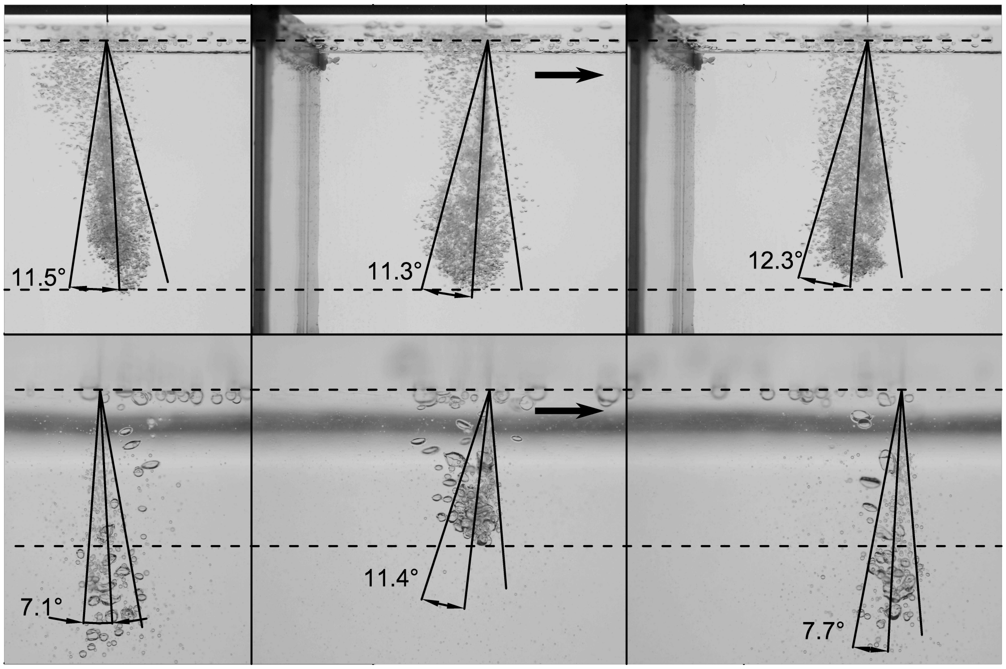

Figure 10: Top line : D = 1.3 mm, V_0 = 18.6 m/s, A = 16 mm, f = 1 Hz, Re = 24137. Bottom line : D = 0.3 mm, V_0 = 9.8 m/s, A = 12 mm, f = 1 Hz, Re = 2950. Left column shows the bubble cloud when the jet reaches its leftmost position. Center column shows the jet reaching its maximum velocity while travelling rightwards. Right column shows the bubble cloud when the jet has reached the rightmost position. The angle α is illustrated for each bubble cloud : this angle is constant for the conditions of the top line, but varies strongly for the conditions of the bottom line, leading to a decrease in the instantaneous penetration depth when horizontal velocity is the largest.

inertia (much smaller Re), it will display a much larger local penetration depth at its outermost positions, where its mixing layer angle is the smallest, and therefore a larger average penetration depth H.

3.2.4. Shape of the bubble cloud

While results of figures 4 to 9 were devoted to measurements of the average penetration depth H of the bubble cloud, a consequence of the previous discussion is that the *local* penetration depth H_{loc} is actually not uniform over the region covered by the oscillating jet. This can be illustrated by superposing instantaneous images of the clouds, see figure 11. The depth of the bubble cloud exhibits strong spatial variations for V_0 = 2.9 m/s and f = 10 Hz, figure 11a,

Table 4: Impact of mixing layer angle α on model penetration depth H_1.

α(°)	10	11.5	12.5	14
H_1 in mm (V_0 = 18.6 m/s, D = 1.3 mm)	315	275	253	226
H_1 in mm (V_0 = 9.8 m/s, D = 0.3 mm)	38	33	30	27

with a minimum at the central location. The same effect is observed, to a smaller extent, for figures 11b and 11c. For the conditions of figure 11d though, corresponding to the same amplitude but to a smaller frequency $f = 1$ Hz, such a minimum at the center is not observed.

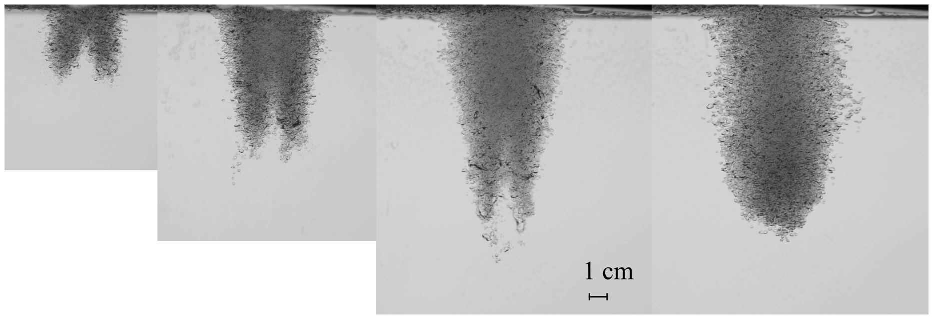

(a) V_0=2.9 m/s f=10 Hz (b) V_0=5.0 m/s f=10 Hz (c) V_0=7.2 m/s f=10 Hz (d) V_0=7.2 m/s f=1 Hz

Figure 11: Global shape of the bubble cloud obtained by superposing images below the oscillating jet. Fixed $D = 2.4$ mm and oscillation amplitude $A = 16$ mm.

The fact that the minimum at the center of the cloud disappears when frequency is lowered can be interpreted via the impact of the effective angle β, illustrated in figure 7 : for conditions of large frequency and hence large β, H_{loc} will decrease when the jet reaches its maximum velocity, namely at the center. Patterns such as those of figures 11a to c are therefore expected to occur for large values of β. A second necessary condition is that the amplitude of the motion must be larger than the width of the instantaneous cloud itself. The width of the cloud at its bottom can be estimated from DV_0/U_T, the condition is then simply that dimensionless number AU_T/DV_0 must be large enough. In the dimensional analysis, this parameter replaces parameter A/D introduced in section 3.2.1, and whose impact had not yet been discussed. We represent on figure 12 a histogram of all our data points, with axes β and AU_T/DV_0. Conditions for which there is a maximum at the center (e.g. figure 11d) are colored in blue, and conditions for which there is on the contrary a *minimum* at the center (e.g. figure 11a) are colored in orange. We consider that there is a minimum at the center when $H_{loc}(\text{max})/H_{loc}(\text{center}) > 1.05$. Figure 12 shows that there is very little overlap of the blue/orange regions, and that the two dimensionless numbers we propose are relevant to predict the shape of the bubble cloud generated by an oscillating jet : spatial heterogeneity of the penetration depth clearly corresponds to larger AU_T/DV_0 and β values. Note that this cartography has been obtained by varying *independently* A, f, V_0, and D, i.e. all the physical parameters introduced in both dimensionless groupings except U_T.

4. Conclusion

We have measured the penetration depth of the bubble cloud generated by an oscillating liquid jet. We have shown that the order of magnitude of the average penetration depth can be well estimated by the simple model of Clanet

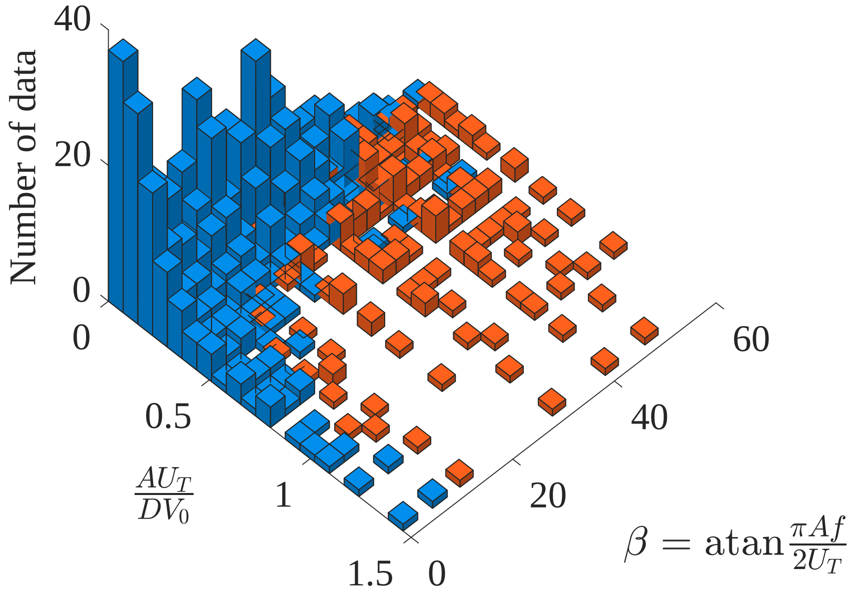

FIGURE 12: Histogram of all data points as a function of AU_T/DV_0 and β (in °), showing in blue conditions for which there is a maximum in penetration depth at the center of the bubble cloud (e.g. figure 11d) and in orange conditions for which there is a local minimum in penetration depth at the center (e.g. figure 11a). A minimum of penetration at the center is observed for larger values of AU_T/DV_0 and β.

& Lasheras (1997) for a non-oscillating tilted jet, with a constant mixing layer angle $\alpha = 12.5°$. The effect of an oscillation of amplitude A and frequency f can be captured via an effective inclination angle $\beta = \mathrm{atan}(\pi A f/2U_T)$. When frequency is varied, a maximum of penetration depth can be observed if the inertia of the jet is low enough, namely if $Re = DV_0/\nu < 10^4$: this maximum is caused by the modification of the ascending flow around the bubble cloud, which impacts the mixing layer angle α. The existence of this maximum, which is not captured by the Clanet and Lasheras (1997) model, is the main cause of discrepancy between experiments and model, up to 30% for β in the range [0.15-0.25].

Examination of the dynamics of the oscillated jet shows that for lower inertia jets, the angle α varies strongly during the course of an oscillation : α is larger at the central position, and smaller at the outermost positions. The local penetration depth is therefore smaller at the central position, and larger at the edges. A consequence of these variations of α, is that for these conditions the global shape of the bubble cloud itself displays a minimum at the central position for large β and AU_T/DV_0. The cartography we provide on figure 12 can be used to predict this shape.

The distance h between the nozzle and the surface is equal to $20D$ for all our measurements. A variation of this distance is expected to affect the amplitude of perturbations on the liquid jet surface when it hits the pool, and therefore the amount of gas entrained below the surface. Preliminary measurements have shown that the quantity of bubbles had little effect on the penetration depth, and only played a part via the secondary flow of ascending bubbles. However, this will have to be quantified more precisely in future experiments.

The penetration depths measured in the present study were obtained for turbulent jets, but the scale of the liquid jets remained small compared to the scales involved in hydraulic systems. As mentioned in the introduction, for larger systems the jet is expected to exhibit natural oscillations related to the development of instabilities along its fall, and it may also fragment. The model presented in this work for the penetration depth is expected to apply as well for such systems provided the oscillation and jet structure at impact are adequately quantified. This will have to be demonstrated in future works.

Acknowledgements

The authors acknowledge the help of Jean Berard on the experimental set-up. The laboratory LEGI is part of the LabEx Tec 21 (Investissements d'Avenir-Grant Agreement No. ANR-11-LABX-0030).

Références

Biń, A. K. (1993). Gas entrainment by plunging liquid jets. *Chem. Eng. Sci.*, *48*, 3585–3630. doi :10.1016/0009-2509(93)81019-R.

Chanson, H., Aoki, S., & Hoque, A. (2006). Bubble entrainment and dispersion in plunging jet flows : Freshwater vs. seawater. *Journal of Coastal Research*, *22*, 664–677.

Clanet, C., & Lasheras, J. C. (1997). Depth of penetration of bubbles entrained by a plunging water jet. *Phys. Fluids*, *9*, 1864. doi :10.1063/1.869336.

Deike, L., Melville, W. K., & Popinet, S. (2016). Air entrainment and bubble statistics in breaking waves. *J. Fluid Mech.*, *801*, 91–129. doi :10.1017/jfm.2016.372.

Descloux, S., Chanudet, V., Taquet, B., Rode, W., Guédant, P., Serça, D., Desmukh, C., & Guerin, F. (2016). Efficiency of the nam theun 2 hydraulic structures on water aeration and methane degassing. *Hydroécol. Appl.*, *19*, 63–86. doi :10.1051/hydro/2015002.

Van de Donk, J. A. C. (1981). *Water aeration with plunging jets*. Ph.D. thesis TU Delft.

Duarte, R., Pinheiro, A., & Schleiss, A. J. (2016). An enhanced physically based scour model for considering jet air entrainment. *Engineering*, *2*, 294–301. doi :10.1016/J.ENG.2016.03.003.

Ervine, D. A., Falvey, H. T., & Withers, W. (1997). Pressure fluctuations on plunge pool floors. *J. Hydraul. Res.*, *35*, 257–279. doi :10.1080/00221689709498430.

Falvey, H. T., & Ervine, D. A. (1987). Behaviour of turbulent water jets in the atmosphere and in plunge pools. *ICE Proc.*, *83*, 295–314. doi :10.1680/iicep.1987.353.

Guyot, G., Rodriguez, M., Pfister, M., Matas, J.-P., & Cartellier, A. (2016). Experimental study of large scale plunging. In B. Crookston, & B. Tullis (Eds.), *Hydraulic Structures and Water System Management. 6th IAHR International Symposium on Hydraulic Structures* (pp. 195–208). doi :10.15142/T3540628160853.

Horn, G., & Thring, M. W. (1956). Angle of spread of free jets. *Nature*, *178*, 205–206. doi :10.1038/178205a0.

Kiger, K. T., & Duncan, J. H. (2012). Air-entrainment mechanisms in plunging jets and breaking waves. *Annu. Rev. Fluid Mech.*, *44*, 563–596. doi :10.1146/annurev-fluid-122109-160724.

Ma, J., Oberai, A. A., Drew, D. A., Lahey, R. T. J., & Moraga, F. (2010). A quantitative sub-grid air entrainment model for bubbly flows - plunging jets. *Computers & Fluids*, *39*, 77–86. doi :10.1016/j.compfluid.2009.07.004.

Maxworthy, T., Gnann, C., Kürten, M., & Durst, F. (1996). Experiments on the rise of air bubbles in clean viscous. *J. Fluid Mech.*, *321*, 421–441. doi :10.1017/S0022112096007781.

McKeogh, E. J., & Ervine, D. A. (1981). Air entrainment rate and diffusion pattern of plunging liquid jets. *Chem. Eng. Sci.*, *36*, 1161–1172. doi :10.1016/0009-2509(81)85064-6.

Miwa, S., Moribe, T., Tsutsumi, K., & Hibiki, T. (2018). Experimental investigation of air entrainment by vertical plunging liquid jet. *Chem. Eng. Sci.*, *181*, 251–263. doi :10.1016/j.ces.2018.01.037.

Nakasone, H. (1987). Study of aeration at weirs and cascades. *J. Environ. Eng.*, *113*, 64–81. doi :10.1061/(ASCE)0733-9372(1987)113:1(64).

Ohkawa, A., Kusabiraki, D., Shiokawa, Y., Sakai, N., & Fujii, M. (1986). Flow and oxygen transfer in a plunging water jet system using inclined short nozzles and performance characteristics of its system in aerobic treatment of wastewater. *Biotechnology and Bioengineering*, *28*, 1845–1856.

Pagliara, S., Palermo, M., & Carnacina, I. (2011). Scour process due to symmetric dam spillways crossing jets. *International Journal of River Basin Management*, *9*, 31–42. doi :10.1080/15715124.2010.549090.

Pope, S. B. (2000). *Turbulent Flows*. Cambridge University Press.